Mission Profile Based System-Level Reliability Analysis of DC/DC Converters for a Backup Power Application

Dao Zhou, *Member, IEEE*, Huai Wang, *Senior Member, IEEE*, and Frede Blaabjerg, *Fellow, IEEE*

***Abstract*—Reliability analysis is an important tool for assisting the design phase of a power electronic converter to fulfill its life-cycle specifications. Existing converter-level reliability analysis methods have two major limitations: 1) being based on constant failure rate models; and 2) lack of consideration of long-term operation conditions (i.e., mission profile). Although various studies have been presented on power electronic component-level lifetime prediction based on wear-out failure mechanisms and mission profile, it is still a challenge to apply the same method to the reliability analysis of converters with multiple components. Component lifetime prediction based on associated models provides only a B_X lifetime information (i.e., the time when $X\%$ items fail), but the time-dependent reliability curve is still not available. In this paper, a converter-level reliability analysis approach is proposed based on time-dependent failure rate models and long-term mission profiles. Two different methods to obtain the component-level time-to-failure are illustrated by a case study of dc/dc converters for a 5 kW fuel cell-based backup power system. The reliability analysis of the converters with and without redundancy is also performed to assist the decision making in the design phase of the fuel cell power conditioning stage.**

***Index Terms*—Capacitor, fuel cell system, power semiconductor, reliability block diagram, system-level reliability, Weibull distribution.**

I. Introduction

FUEL cells are widely recognized as one of the most promising alternative power conversion technologies due to their high efficiency, and they provide very low pollution [1], [2]. In addition, the scalability of fuel cells allows extensive applications from low power to high power [3]. For instance, fuel cells have progressed from being a potential technology to a commercially viable power solution for mobile base stations [4]. As telecom backup power systems are typically located in remote areas with harsh environments, frequent interruptions of the electrical grid place a high priority on the availability and reliability of the total system. As stated in [5], the reliability is the probability that a product can perform a required function under given conditions for a given time interval. The failure rate of a product, such a bathtub curve, consists of three major stages in its entire life cycle [6]: a decreasing failure rate caused by early infant mortality, a constant failure rate due to random failure, and an increasing failure rate because of the wear-out phenomenon. To design a backup power system to fulfill a certain service life, the failure due to component wear-out should be avoided or limited to an acceptable level.

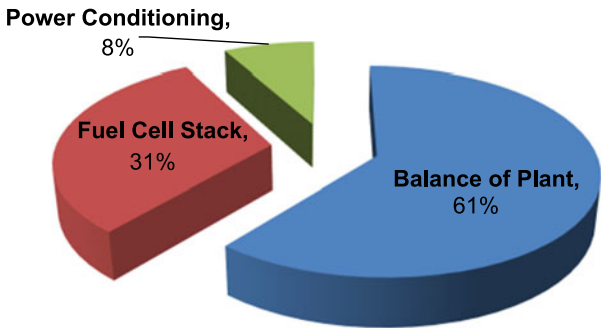

Fig. 1. Outage frequency of the subsystems in proton exchange membrane fuel cell power plants.

According to a field study of residential-scale proton-exchange-membrane (PEM) fuel cell power plants (1–5 kW) [7], the most prevalent means of failure in fuel cell systems are distributed as shown in Fig. 1. They are categorized from the fuel cell stack, power conditioning stage, and balance of the plant. Insight into the component-level durability and reliability of these subsystems of fuel cell systems are investigated in [7]–[9], especially for the fuel cell stack and the balance of the plant given their high outage frequency. In [7], the component failure is statistically analyzed based on a fleet of deployed PEM fuel cells, and the critical components can be identified with the recorded average lifetime. Unfortunately, the root cause of the failure mechanism cannot be identified by using this approach. In addition, it cannot easily evaluate the significant cause of the failures owing to the varying climate and operating conditions at the installation sites. Various efforts have been made to investigate the degradation mechanisms of fuel cell components to enhance durability [8], [9]. However, a quantitative lifetime model with respect to a certain stressor of these components is lacking, which clearly affects the accurate reliability assessment of fuel cells facing different mission profiles. The reliability

Manuscript received May 8, 2017; revised August 15, 2017; accepted October 26, 2017. Date of publication November 1, 2017; date of current version June 22, 2018. This work was supported by the Innovation Fund Denmark through the Advanced Power Electronic Technology and Tools Project. Recommended for publication by Associate Editor D. Xu. *(Corresponding author: Dao Zhou.)*

The authors are with the Department of Energy Technology, Aalborg University, Aalborg 9220, Denmark (e-mail: zda@et.aau.dk; hwa@et.aau.dk; fbl@et.aau.dk).

Color versions of one or more of the figures in this paper are available online at http://ieeexplore.ieee.org.

Digital Object Identifier 10.1109/TPEL.2017.2769161

evaluation of the power conditioning stage is the main topic of this paper, which starts from the analysis of the critical components in the system. According to an industry survey [10], [11], the power semiconductors and capacitors are two types of fragile elements in the power electronics converter. Magnetic devices have potential reliability issues when applied in high-density power converters (i.e., thermal related degradation) or medium- to high-voltage applications (e.g., insulation degradation). For most of other applications, the thermal-related or insulation-related degradation is negligible for magnetic devices. Moreover, among the various stressors (vibration, humidity, temperature, etc.) for electronic equipment, temperature contributes up to 55% of the failure distribution [12]. Several research efforts have been devoted to the reliability prediction of electronic equipment [13]–[19]. On the one hand, the failure rate determined by using exponential distribution is adopted from various handbooks [13], [14]. This method is simple and inappropriate, considering only the operation period with a constant failure rate but neglecting the wear-out. On the other hand, the thermal stress of the critical components can be obtained according to the mission profile of the power converter used in renewable energy systems [15]–[19]. However, owing to the particular characteristics of the backup power application, this physics-of-failure-based reliability evaluation cannot be performed with frequent switching between the standby mode and operation mode.

Based on the component-level reliability metrics, the system-level reliability can instead be derived by using the Reliability Block Diagram (RBD), the Fault Tree Analysis (FTA), and the Markov Chain (MC) [20]–[27]. In [20]–[22], the reliability of an interleaved dc/dc boost converter, an induction motor drive, and a PEM fuel cell power plant are evaluated using the MC method. In addition, the RBD approach is used to analyze the reliability of a paralleled inverter system [23] and a multilevel converter [24]. However, a constant failure rate is applied in both situations, which neglects the effects introduced by the mission profile. An FTA for the PEM fuel cell is performed in [25], where again a constant failure rate is assumed. Moreover, the most fundamental difference is that the success combination is focused in the RBD, whereas the failure combination is considered in the FTA. In other words, an FTA can easily be converted into an RBD, because the FTA analyzes the fixed probabilities (i.e., each event that comprises a tree has a fixed probability of occurring) and the RBD may include time-varying distribution for success and other properties [28]. However, this research very seldom considers the mission profile.

The background of this paper is related to a 5 kW commercial fuel cell system for backup power. It is an application requiring high reliability (i.e., 0.99) within a service life of 5 years. The motivation is to predict the reliability of the power conditioners (i.e., dc/dc converter stage) at the end of service life to better size the key electronic components for the next generation product design. The outcome for the study is used to assist the design phase of product development. The novel aspects of the proposed method of reliability evaluation are as follows: 1) consider long-term (i.e., one year) mission profile (i.e., environmental conditions, occurrence of power grid outages, standby mode, and active mode), and 2) obtain the lifetime distribution of power MOSFETs and capacitors using Monte Carlo analysis and the degradation testing data to consider the parameter variations in both components and lifetime models.

The rest of the paper is organized as follows: Section II describes the mission profile and the topology of the fuel cell power converter used in the backup power application. Sections III and IV address the way to obtain the time-to-failure of the power semiconductors and the capacitors. Section V considers the reliability of the whole power stage by using the RBD and concluding remarks are drawn in the last section.

II. Description of Power Stage for Backup Power Application

The most commonly used technologies for backup power systems in telecom applications are lead-acid battery systems and generator sets. PEM fuel cells are emerging as an important alternative, because of their low operation temperature, and relatively fast response time [4]. Compared to batteries, fuel cells provide longer continuous runtime and greater durability in outdoor environments under a wide range of temperature conditions. They require less maintenance than either generators or batteries because they have fewer moving parts. Because of the ac output of the generator and the variable dc output of the fuel cell, a power conversion unit is evitable in these two cases. In addition, power electronics are needed to charge the batteries and control the loading current. However, the loading stresses of the power electronic components are different owing to various output characteristics of the batteries, generators, and fuel cells.

The fuel cell system consists of three subsystems: the balance of plant regulates the pressure of fuel and air, and maintains the fuel cell at a reasonable temperature by controlling the coolant loop. The fuel cell stack converts the chemical energy into electricity through an electrochemical reaction. Afterward, a power stage is applied to provide a stable dc-bus used in telecom applications from the varying stack output voltage.

A. Description of Mission Profile

Regarding the backup power, two major working modes can be identified. The power converter mainly works in the standby mode when the power grid is operational, whereas the power converter sometimes works in the operation mode in the case of a power outage.

The annual ambient temperature with a sample rate of one day is shown in Fig. 2(a), and it can be distributed into different temperature ranges. As shown in Fig. 2(b), the stability of the power grid is an essential mission profile, and daily outage with 4-h duration, which determines the operation period of the fuel cell system, can be expected for severe users [29]. Meanwhile, the loading profile of the telecom application is repeated with a 10-h quarter load and 2-h full load, as stated in [4]. Moreover, the input of the power stage, determined by the *V–I* characteristics of the fuel cell stack, is shown in Fig. 2(c).

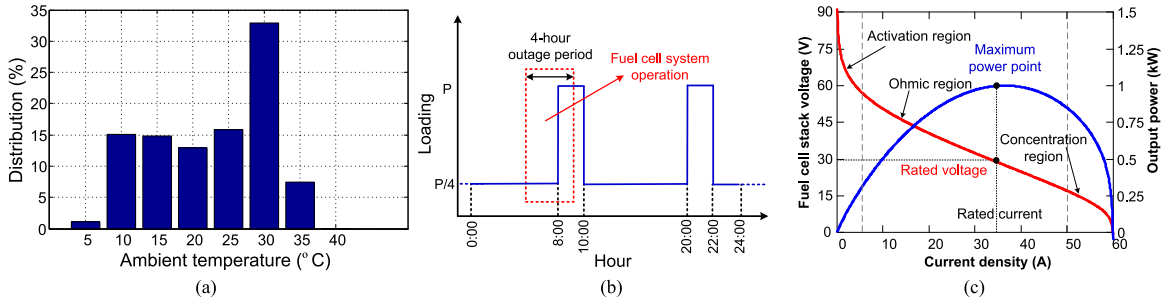

Fig. 2. Annual mission profile of telecom power. (a) Temperature distribution with a sample rate of one day. (b) Loading profile of the telecom application and operation period of the fuel cell system. (c) Output voltage and power of a fuel cell in relationship with current density.

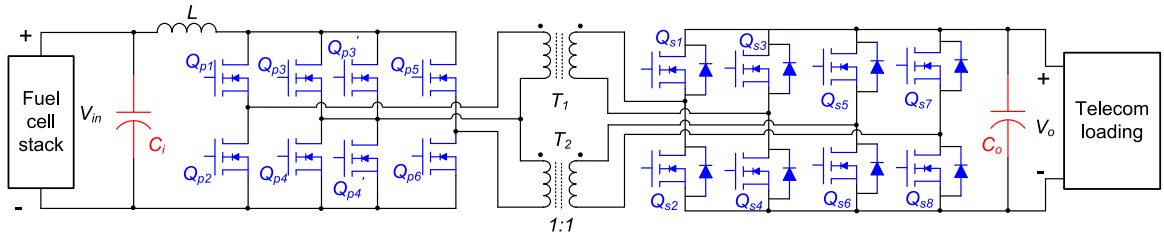

Fig. 3. Topology of isolated 1 kW dc/dc power converter used in a fuel cell backup telecom power.

TABLE I
POWER CONVERTER SPECIFICATION AND PARAMETERS

Input voltage $V_{\rm in}$	30 – 65 V
Output voltage V_o	48 V
Maximum output power P_o	1000 W
Primary-side MOSFETs	100 V/74 A, × 8
Secondary-side MOSFETs	100 V/74 A, × 8
Input capacitor C_i	390 μF/100 V, × 6
Output capacitor C_o	680 μF/63 V, × 8
Input inductor L	15 μH
Transformer ratio n	1:1
Switching frequency $f_{\rm sw}$	50 kHz

B. Structure of Power Converter

Due to the variable output voltage of the fuel cell stack, a dc/dc power converter is required to match the voltage in telecom applications. A topology using galvanic isolation is shown in Fig. 3, where the rated power of the converter is 1 kW, and six 1 kW converters are connected in parallel for a 5 kW power stage to obtain the redundancy. Moreover, a synchronous rectification is adopted to achieve low conduction losses in the situation of low voltage and high current at the secondary side of the transformer [29].

The specification and main parameters of the 1 kW power converter are listed in Table I. As the power semiconductors and dc capacitors are the major reliability critical components in the power electronic converter, their performance will be evaluated and discussed in detail as follows.

III. TIME-TO-FAILURE OF POWER SEMICONDUCTORS

This section addresses the method to estimate the time-to-failure of the power semiconductors. It starts with the B_{10} lifetime due to the limited lifetime data, which means that 10% of a sample will fail at this operation time. It can then be further extended to a lifetime distribution, if the parameter deviations are taken into account.

A. B_{10} Lifetime Estimation

As shown in Fig. 3, since the reflected voltage of the transformer primary side can be higher or lower than the voltage of the fuel cell, the power converter can operate in both the step-up mode and the step-down mode [29]. In the case of step-up mode, the primary-side inductor is charged by the activation of all transistors, and it is discharged by the parallel connection of the two transformers. As described in [26], because the transistors in the middle bridge carry double of the current compared to the side bridges, two MOSFETs Q_{p3} and Q_{p4} are connected in parallel to realize the balanced loading among the bridges of the primary side. In the case of the step-down mode, the inductor is charged by the parallel connection of the transformers, and it is discharged by the series connection of the transformers. This results in a variable loading of the transistors among the bridges in the primary side.

At the primary side, although the loading of the transistors is unbalanced among the different bridges, owing to the symmetrical loading of the upper and lower transistors, only Q_{p1}, Q_{p3}, and Q_{p5} are chosen. In addition to the symmetrical loading of the upper and lower transistors, the two rectifiers share the same current and voltage loading. As a result, Q_{s1} can represent the loading at the secondary side.

The power semiconductor reaches the end-of-life when an overlap occurs between its stress level and the strength model. From the power cycling perspective, the stress analysis is related to the mission profile (e.g., the ambient temperature, the loading profile, and the grid availability), whereas the strength model is determined by the selection of the power device and associated cooling. As discussed in [31], although the approach to evaluate

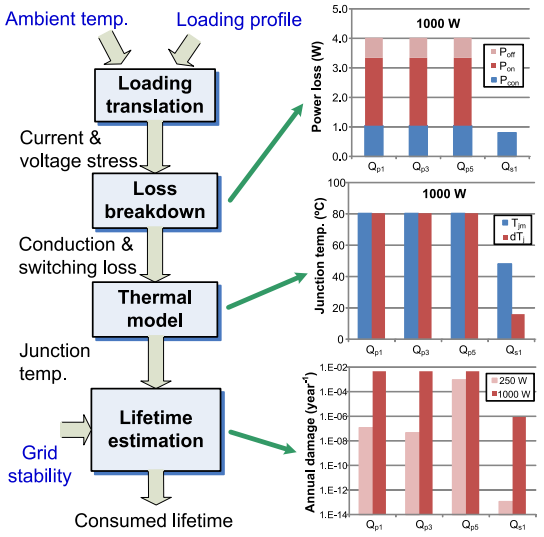

Fig. 4. Flowchart to predict lifetime of power semiconductor in the operation mode.

the thermal stress of the power semiconductor at the standby mode and the operation mode is different, only the operation mode is considered, because much higher junction temperature leads to the dominating lifetime consumption compared to the standby mode.

The flowchart to predict the lifetime of the power semiconductor in the case of the operation mode is shown in Fig. 4. Under this circumstance, the junction temperature of the power semiconductor is jointly determined by the ambient temperature and the loading profile. The loss distribution of the MOSFET mainly consists of the conduction loss $P_{\rm con}$ and the switching loss, which can be further divided into the turn-on losses $P_{\rm on}$ and the turn-off losses $P_{\rm off}$. The loss calculation of the MOSFET is consistent with Infineon application note [32], and the key waveforms of each MOSFET at different loading conditions during a switching period are discussed in detail [31]. Owing to the discrete MOSFET, its own heat-sink results in an independent thermal system, and a thermal coupling can be neglected from the adjacent devices. Considering an ambient temperature of 40 °C as the worst-case scenario, the mean junction temperature T_{jm} and the junction temperature fluctuation dT_j can be calculated, based on the thermal impedance from the junction to the ambient.

Regarding the lifetime model of the MOSFET, a discrete component is selected due to the low power rating of the converter and the cost. The chip die is soldered onto the copper base, and the bonding pads and die-attach are common failure mechanisms [33], [34], which are almost the same as the cases when the IGBT power module is applied [35], [36].

Due to the limited published power cycling data of the discrete MOSFETS [33], the lifetime model is consistent with the one mentioned in [34]. Compared with Bayerer's lifetime model [35]–[37], the insignificant impacts from the mean junction temperature and on-time pulse duration are not considered, so the cycle-to-failure N_f can be expressed as

$$N_f = A \cdot dT_j^{\beta_1} \tag{1}$$

TABLE II
EQUIVALENT STATIC VALUE FOR EACH MOSFET

	Q_{p1}	Q_{p3}	Q_{p5}	Q_{s1}
Number of cycles per year n	365	365	365	365
Annual damage D (year^{-1})	5.20E–3	5.20E–3	6.30E–3	2.87E–6
Number of cycles to failure N_f	7.02E4	7.02E4	5.79E4	1.27E8
Mean junction temperature T_{jm} (°C)	62.5	61.0	102.7	43.3
On-state time $t_{\rm on}$ (second)	14 400	14 400	14 400	14 400
Junction temperature fluctuation dT_j (°C)	83.9	85.5	54.4	14.4

where the power cycle is closely related to the junction temperature swing. In addition, A and β_1 can be obtained according to test data provided by [34]. Owing to small manufacturing variations of the devices, it is impossible to exactly predict the wear-out process when an individual device will fail. The only meaningful values are the failure probability for an individual device and the percentage of failed devices for entire populations. It is worth noting that these data are aimed for the B_{10} lifetime, which means that 10% of the sample fails when the power cycling reaches this number.

Together with the thermal profile of the power semiconductors, the cycle-to-failure can be calculated in the conditions of the full load and the quarter load, respectively. On the other hand, the annual power cycling of each loading condition can be estimated with the grid outage frequency. Based on Miner's rule [38], [39], the annual damage $D_{\rm MOS}$ can be calculated by the annual power cycling n over the corresponding end-of-life power cycles

$$D_{\rm MOS} = \sum \frac{n(i)}{N_f(i)} \tag{2}$$

where i indicates different loading conditions like the full load and the quarter-load.

B. Time-to-Failure of Individual Power Semiconductor Due to Parameter Deviation

The previous discussion gives a B_{10} annual damage of MOSFETs used in a power converter, but the uncertainties due to the statistic properties of the applied lifetime model and the parameter variations of the power device should also be taken into account. Therefore, a statistical approach to analyze the lifetime performance subject to parameter variations is carried out in detail by means of Monte Carlo analysis. Finally, the time-to-failure distribution of the power semiconductors can be estimated by considering the parameter variations.

Since the lifetime model is obtained from the accelerated test results based on a specific number of testing samples, there are uncertainties in the derived constant parameters. All parameters in the lifetime model as stated in (1) are distributed by means of a normal probability density function (pdf), assuming that A and β_1 experience a variation of 5%.

It is noted that μ denotes the mean value of the distribution, and σ denotes the standard deviation. To simplify the thermal stress from both the full load and the quarter load, the equivalent

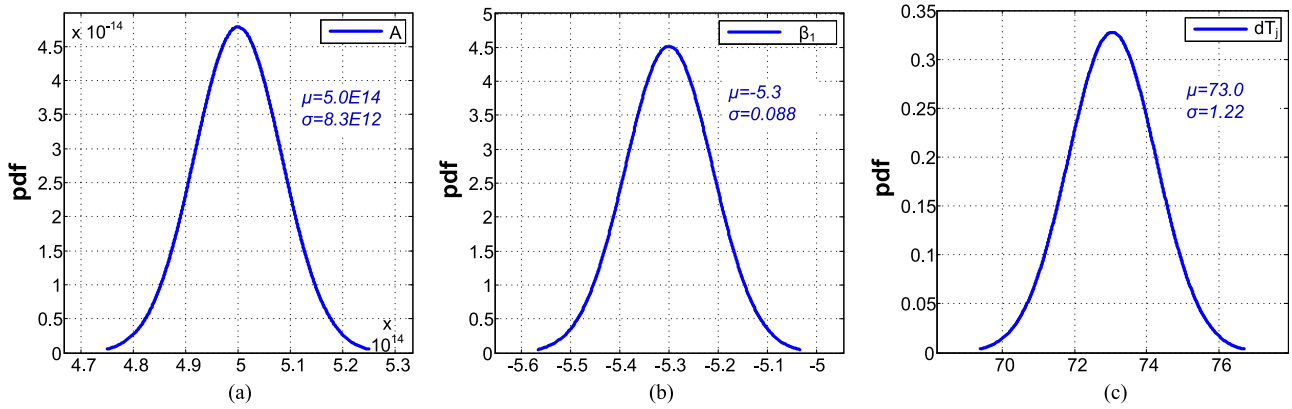

Fig. 5. Normal distribution of the factors from the lifetime model. (a) A—scaling factor. (b) β_1—exponential factor of temperature swing. (c) dT_j—junction temperature fluctuation.

static values of the lifetime data can be calculated as given in Table II.

The second type of uncertainty exists due to variances in the manufacturing process (like the typical, maximum, and minimum on-state resistance of the MOSFET), which results in variation of the mean junction temperature and junction temperature fluctuation. In order to illustrate this, Q_{p5} is selected as an example. As shown in Fig. 5, the junction temperature fluctuation experiences a variation of 5%. Each distribution is sampled by using Monte Carlo analysis, whose sample numbers results in the accuracy of the output distribution [5], [40]. Consequently, [10,000] samplings are chosen to establish the accumulated damage distribution.

In the condition that all parameter variations are taken into account, the annual damage distribution is depicted in Fig. 6(a). It is known that the time-to-failure data typically follow the Weibull distribution [41]:

$$f(t) = \frac{\beta}{\eta}\left(\frac{t}{\eta}\right)^{\beta-1} \cdot \exp\left[-\left(\frac{t}{\eta}\right)^{\beta}\right] \tag{3}$$

where η denotes the scale parameter and β denotes the shape parameter.

As a result, the fitting curve of the annual damage can be obtained with a scale parameter of 6.7E–3 and a shape parameter of 2.60. Assuming that the mission profile is repeated every year, the Weibull distribution of the lifetime, which is defined as one over the annual damage, can be obtained as well. Thus, the unreliability or failure of the power switch Q_{p5} can be calculated as shown in Fig. 6(b), which is the integration of the lifetime distribution. It is noted that 1% of MOSFETs are predicted to fail over more than 30 years.

With the static equivalent values of each component as listed in Table II, the lifetime distributions of the key MOSFETs can be calculated, considering 5% parameter variations from the lifetime model and the stress analysis. Since the scale parameter of the Weibull function denotes the value when 63.2% failure occurs, it is predicted that Q_{p5} has the lowest scale parameter of 220.5 according to the accumulated damage estimation as shown in Fig. 4. For the accumulated failure shown in Fig. 7, it can be seen that the 5-year operation (i.e., desired lifetime of the fuel cell backup power system) results in 5.8E–5, 4.3E–5, and 3.5E–5 failure in Q_{p1}, Q_{p3} and Q_{p5}, respectively.

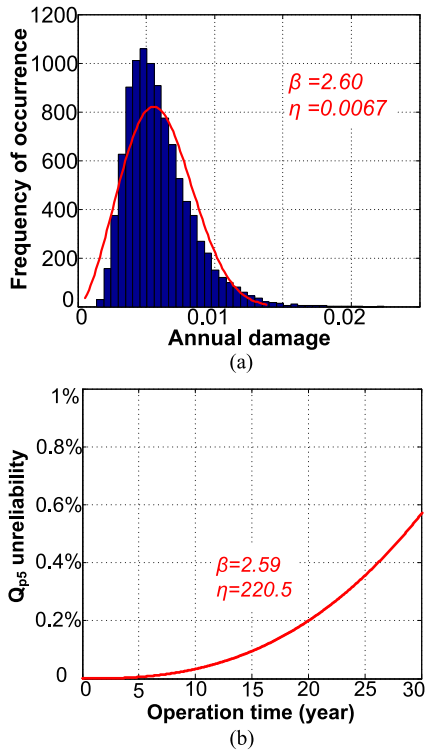

Fig. 6. Monte Carlo analysis considering all parameter variations from the stress evaluation and lifetime model for the most stressed MOSFET Q_{p5}. (a) Annual damage distribution. (b) Accumulated percentage of failure (i.e., unreliability) along with the operation time.

IV. Time-to-Failure of DC Capacitors

Due to the lack of complete failure data, the previous section calculated the B_{10} lifetime of the power semiconductors, and then the lifetime distribution can be obtained by considering the parameter deviations. In this section, the lifetime distribution of the dc capacitors is studied, based on the complete failure data of the capacitors.

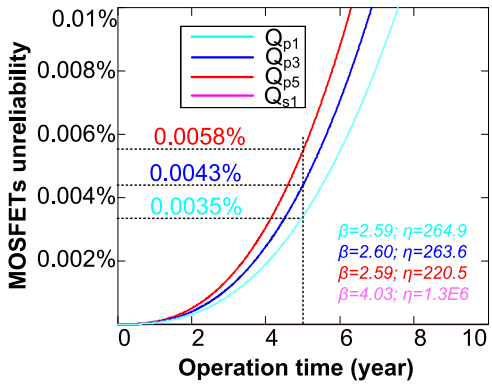

Fig. 7. Monte Carlo analysis of four typical power switches in terms of the accumulated failure.

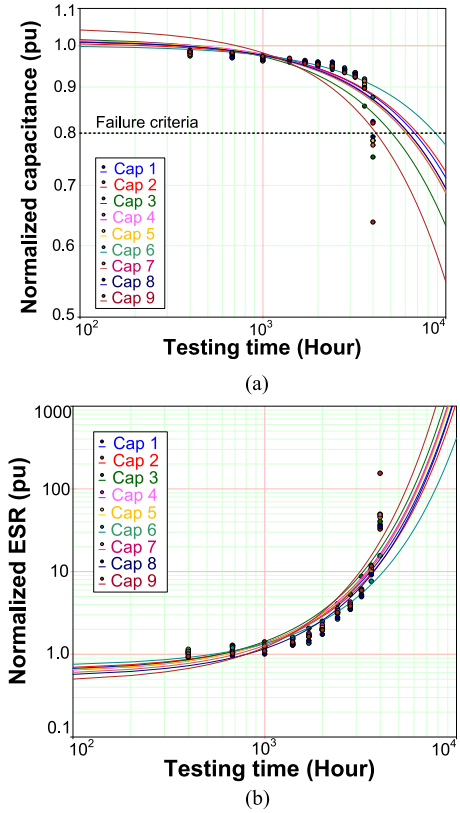

Fig. 8. Capacitor degradation testing results at rated voltage, rated ripple current, and upper category temperature (105 °C). (a) Normalized capacitance. (b) Normalized ESR.

A. Weibull Lifetime Data

The capacity change, dissipation factor, and leakage current are generally considered as key indicators during the healthy condition of the electrolytic capacitors [42]. To obtain the failure statistics of the used capacitor, a degradation test is performed with a series of nine capacitors (56 μF/35 V) at the rated voltage, an upper category temperature (105 °C) and rated ripple current, and the normalized capacitance and equivalent series resistance (ESR) are regularly measured during 4000 testing hours. As shown in Fig. 8, the results are analyzed by using the software tool Weibull++ [41]. It can be observed that during the process

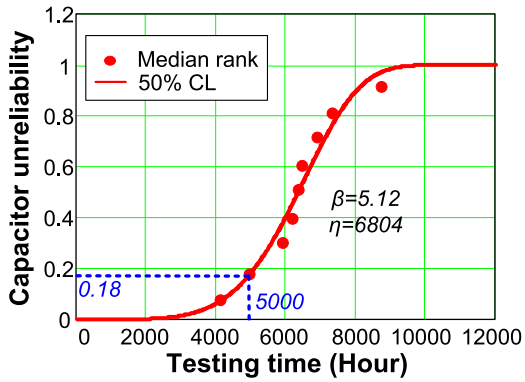

Fig. 9. Time-to-failure of capacitors at 50% confidence levels (CL) by using Weibull distribution using upper category temperature of 105 °C.

of the testing hours, the initial capacitance and ESR increase or decrease smoothly until they reach the turning point after 4000 h. This agrees with the end-of-life criteria of the individual capacitor, which typically is 20% drop of initial capacitance.

Generally, the exact reliability and the probability of the failure can never be known unless the failure data of every unit in the population can be obtained. Since this usually is not a realistic solution, the testing with a certain number of samples is used to estimate the reliability, which introduces the confidence level (CL)—A range within which these reliability values are likely to occur with a certain percentage of time. The widely adopted 50% CL is applied by using median rank [41], where the lifetime is neither overestimated nor underestimated. The time-to-failure of nine samples are located as shown in Fig. 9, and they can be fitted in terms of a Weibull distribution with a shape factor of 5.12 and scale factor of 6804. It can be seen that the claimed lifetime of 5000 h in the datasheet means almost B_{20} lifetime. Moreover, B_X lifetime at any condition can be calculated based on this.

As discussed in [42] and [43], the state-of-the-art lifetime model for the electrolytic capacitors is affected by the temperature stress and the voltage stress, and it is given by

$$L = L_0 \cdot 2^{\frac{T_0 - T}{n_1}} \left(\frac{V}{V_0}\right)^{-n_2} \tag{4}$$

where L_0 and L are the lifetime under the reference condition and the use condition, V_o and V are voltage at reference condition and use condition, and T_0 and T are the temperature at the reference condition and use condition, respectively. n_1 is the temperature dependent constant, and n_2 is the voltage stress exponent. Based on the leading capacitor manufacturers [43], n_2 equals 0 for small radial capacitors (below a rated voltage of 160 V), as the temperature dependent electrolyte loss dominates the lifetime model. For medium or large sizes (snap-in and screw terminal types), the more closely the operating voltage approaches the rated voltage, the more the electrolyte is consumed for self-healing of small flaws within the dielectric layer. In addition, n_1 equals 10 for the analyzed capacitors, which follows the "10-Kelvin-rule" deduced from the Arrhenius law. According to the above equation, the lifetime estimation at other operational temperature stresses can be calculated.

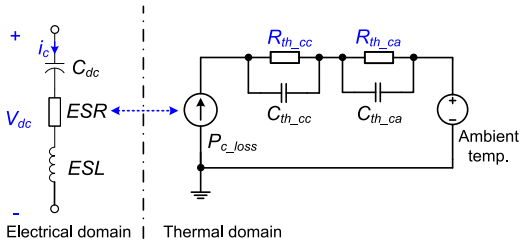

Fig. 10. Relationship between the electrical and thermal models of electrolytic capacitors.

B. Time-to-Failure Distribution of Individual Capacitor

According to the loading condition and thermal model of the electrolytic capacitor, the operation temperature of the capacitor can be calculated in the cases of the standby mode and the operation mode. Afterward, based on the lifetime model of the capacitor, the expected B_X lifetime for the input-side and output-side capacitor can be calculated.

In the case of standby mode, the capacitor temperature is almost the same as the ambient temperature. Based on the ambient temperature distribution and the stability of the power grid, the annual damage can be calculated for each temperature range with the help of the lifetime model listed in (4), which can be accumulated as the total annual damage by using Miner's rule. In the case of the operation mode, the capacitor temperature is jointly determined by the loading condition and the ambient temperature. As shown in Fig. 10, the loss of the capacitor is caused by the ripple current across the ESR, whereas the temperature of the capacitor can be estimated based on the thermal impedance of the capacitor as well as its cooling solutions.

The annual damage of the capacitor D_{cap} is defined as

$$D_{\text{Cap}} = \sum_{i=1}^{7} \frac{P_1 \cdot 365 \cdot 24 \cdot P_2(i)}{L(i)} = \frac{P_1 \cdot 365 \cdot 24 \cdot}{L_0} \sum_{i=1}^{7} \frac{P_2(i)}{2^{\frac{T_0 - T(i)}{10}}} \tag{5}$$

where i indicates the temperature sequence ranging from 5 to 35 °C as shown in Fig. 2(a), P_1 denotes the percentage of the power converter working in the standby/operation mode, P_2 denotes the percentage of the temperature distribution, and L denotes the predicted lifetime at the temperature level, which is the ambient temperature in the case of the standby mode and the sum of the ambient temperature and core temperature rise in the case of the operation mode.

Although the types of input-side and output-side capacitors are different from the tested capacitor, all of them belong to the family of the radial electrolyte capacitor, whose lifetime expectancy is 5000 h as mentioned in their datasheets. Consequently, the lifetime model as shown in Fig. 9 is suitable for both the input capacitor and the output capacitor. Based on the B_{10} and B_1 lifetime model, the damage of the output-side capacitor is shown in Fig. 11, in which the standby mode and the operation mode are compared. Although the loading condition leads to a rise of the capacitor temperature, when the B_{10} lifetime is taken into account, the higher proportion of standby mode causes a higher annual damage of 6.4E-3 compared to the operation mode of 5.2E–3. Meanwhile, if B_1 lifetime model is

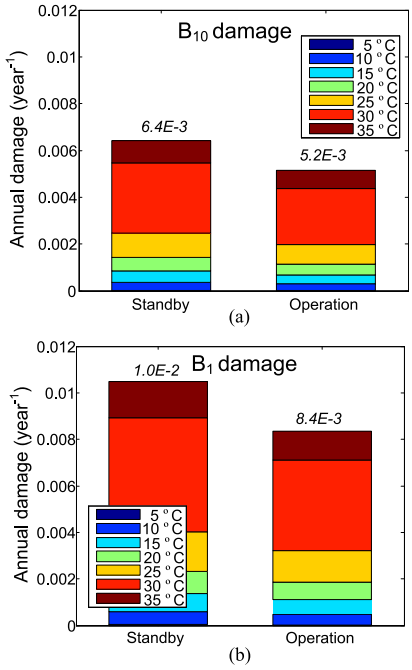

Fig. 11. Annual damage of the output-side capacitor in the case of the standby mode and operation mode. (a) B_{10} damage. (b) B_1 damage.

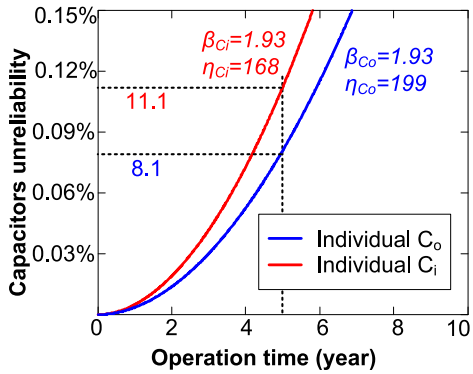

Fig. 12. Time-to-failure of individual input and output capacitors within 10-years of operation.

considered, the annual damage in both the standby mode and the operation mode is higher than that of B_{10} because of its lower cycle-to-failure at the same stress level. Similarly, the same approach can be extended to the input-side capacitor, and B_{10} and B_1 damage can be calculated as well.

With the calculated B_{10} and B_1 lifetime for the input-side capacitor and output-side capacitor, the key Weibull parameters of their time-to-failure curves can be fitted. It is noted that the shape factor and the scale factor for the individual input capacitor are 1.93 and 168, whereas these factors for the individual output capacitor are 1.93 and 199, respectively. Similarly, in the case where the 5-year operation (desired lifetime of the fuel cell power stage) is in focus, the unreliability of the capacitor along with the operation time is shown in Fig. 12. It is evident that 5-year operation of the fuel cell system induces 11.1E–4 and 8.1E–4 failure for the input capacitor and output capacitor, respectively.

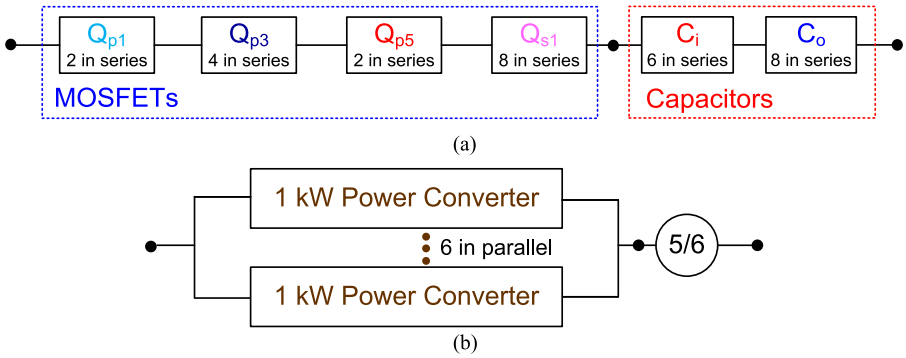

Fig. 13. System-level reliability calculation by using reliability block diagram. (a) Composition of MOSFETs and capacitors in 1 kW power converter. (b) Composition of 5 kW power stage considering redundancy.

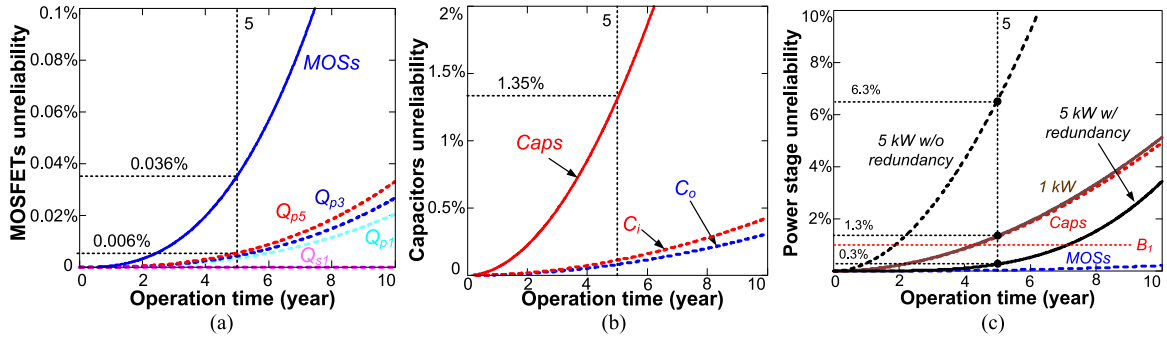

Fig. 14. Accumulated percentage of unreliability from component level to system level. (a) From MOSFETs to 1 kW power converter. (b) From capacitors to 1 kW power converter. (c) From 1 kW power converter to 5 kW power stage with and without redundancy.

V. Reliability Assessment of Power Stage

In order to assess the reliability metrics of the entire power stage in the fuel cell system, major steps can be divided into the reliability analysis of a 1 kW power converter and a 5 kW power stage. By using RBD, the procedure to calculate the reliability function is shown in Fig. 13. It is evident that the reliability evaluation of the total power semiconductors and capacitors is calculated by each component. Afterward, the 5 kW power converter stage can be investigated based on the 1 kW power converter. Due to the same time-to-failure characteristic of the used power devices and dc capacitors, only these components are considered in this paper.

For the reliability analysis of a 1 kW power converter, the existence of any failed MOSFET or capacitor results in abnormal operation of the power converter, which indicates that all MOSFETs and capacitors are serially connected in RBD. As the reliability of the series block is the product of all components, the failure function of subsystem F_{Sub} can be expressed by the component failure function F_{Com} [5]

$$F_{\mathrm{Sub}}(t) = 1 - \prod_{i} \left(1 - F_{\mathrm{Com}(i)}(t)\right). \tag{6}$$

As mentioned before, the MOSFETs are not evenly stressed and the four representing MOSFETs can be found. The reliability of the 1 kW power converter can then be calculated by considering all MOSFETs used in the primary side and secondary side. As shown in Fig. 14(a), the reliability of the total MOSFETs can be deduced from each component. It can be seen that the damage of the 5-year operation (desired lifetime of the backup power) increases from less than 0.01% of the most stressed MOSFET to almost 0.04% of all MOSFETs existed in the 1 kW power converter. Meanwhile, the reliability of the total capacitors from the input capacitor and output capacitor is shown in Fig. 14(b).

The reliability of the whole power stage can be estimated from the reliability analysis of the 1 kW power converter, where six 1 kW power converters are connected in parallel for a 5 kW application. In the case of m-out-of-n redundancy, the failure function of the system F_{Sys} can be expressed as [5]

$$F_{\mathrm{Sys}}(t) = \sum_{i=0}^{m-1} \frac{n!}{i!(n-i)!} \cdot (1 - F_{\mathrm{Sub}}(t))^{i} \cdot F_{\mathrm{Sub}}(t)^{n-i}. \tag{7}$$

The unreliability of the whole power stage is shown in Fig. 14(c), where the cases with and without redundancy are compared as well. Due to the fact that five reliability blocks are serially connected in the condition without redundancy, the lifetime of the power stage is significantly reduced compared to the 1 kW power converter. However, in the case of using redundancy, the reliability of the power stage can be enhanced compared with no redundancy. It can be seen that the accumulated damage reaches 1% (i.e., R = 0.99) for approximately 2 years of the power stage without redundancy, whereas it can be enhanced to 7.5 years with $N+1$ redundancy. It is noted that 5-year operation results in 1.3% failure of the 1 kW power converter, whereas it has 0.3% and 6.3% failure whether the redundancy is applied. It is concluded that, in order to achieve the high reliability (i.e., 0.99) within a service life of 5 years,

the *N+1* configuration must be employed. Alternatively, it can be achieved by sizing the dc capacitors to be more reliable.

VI. Conclusion

A system-level reliability analysis method of dc/dc converters for the power conditioning stage of a fuel cell stack is proposed in this paper. Mission profile and Weibull distribution-based analysis are applied by using the long-term electrothermal stress profiles and the time-to-failure distribution of key components. A case study of an industrial designed 5 kW fuel cell system with multiple dc/dc converters is presented. The reliability curves of the MOSFETs and capacitors used in the dc/dc converters is predicted by considering the associated electrothermal loadings and statistical properties in lifetime models and component parameters. The unreliability of the group for 16 MOSFETs and the group of 14 capacitors reaches 1% when the single dc/dc converter operates 18 years and 4.5 years, respectively. Without redundancy, it will last only 2 years for the power conditioning stage with five paralleled 1 kW dc/dc power converters. To extend its lifetime, a redundant design with additional 1 kW dc/dc converter is analyzed and the operational time is increased to 7.5 years, which fulfills the high reliability demands (i.e., 0.99) for a service life of 5 years. Although the study case is carried out in a fuel cell application, a general approach is to evaluate the system-level reliability. By knowing the mission profile, and the thermal stress and lifetime distribution of the critical components, the reliability of the power converter used in popular applications (e.g., renewable energy system, drive system) can be investigated in a similar way.

References

[1] K. Rajashekara, "Hybrid fuel-cell strategies for clean power generation," *IEEE Trans. Ind. Appl.*, vol. 41, no. 3, pp. 682–689, May 2005.

[2] H. Tao, J. L. Duarte, and M. A. M. Hendrix, "Line-interactive UPS using a fuel cell as the primary source," *IEEE Trans. Ind. Electron.*, vol. 55, no. 8, pp. 3012–3021, Aug. 2008.

[3] X. Yu, M. R. Starke, L. M. Tolbert, and B. Ozpineci, "Fuel cell power conditioning for electric power applications: A summary," *IET Elect. Power Appl.*, vol. 1, no. 5, pp. 643–656, Sep. 2007.

[4] M. J. Vasallo, J. M. Andujar, C. Garcia, and J. J. Brey, "A methodology for sizing backup fuel-cell/battery hybrid power systems," *IEEE Trans. Ind. Electron.*, vol. 57, no. 6, pp. 1964–1975, Jun. 2010.

[5] P. D. T. O'Connor and A. Kleyner, *Practical Reliability Engineering*, 5th ed. New York, NY, USA: Wiley, 2012.

[6] G. A. Klutke, P. C. Kiessler, and M. A. Wortman, "A critical look at the bathtub curve," *IEEE Trans. Rel.*, vol. 52, no. 1, pp. 125–129, Mar. 2003.

[7] S. Lux, K. Johnson, and N. Josefik. "Component failure analysis from a stationary proton exchange membrane fuel cell demonstration," *J. Fuel Cell Sci. Technol.*, vol. 9, no. 5, pp. 1–7, 2012.

[8] F. A. de Bruijn, V. A. T. Dam, and G. J. M. Janssen, "Review: Durability and degradation issues of PEM fuel cell components," *Fuel Cells*, vol. 8, no. 1, pp. 3–22, 2008.

[9] J. Wu *et al.*, "A review of PEM fuel cell durability: Degradation mechanisms and mitigation strategies," *J. Power Sources*, vol. 84, no. 1, pp. 104–119, 2008.

[10] E. Wolfgang, "Examples for failures in power electronics systems," in *Proc. ECPE Tut., Rel. Power Electron. Syst.*, Nuremberg, Germany, Apr. 2007, pp. 1–10.

[11] S. Yang, A. T. Bryant, P. A. Mawby, D. Xiang, L. Ran, and P. Tavner, "An industry-based survey of reliability in power electronic converters," *IEEE Trans. Ind. Appl.*, vol. 47, no. 3, pp. 1441–1451, May 2011.

[12] *Handbook for Robustness Validation of Automotive electrical/electronic Modules*, ZVEI, Frankfurt, Germany, 2008, pp. 1–44.

[13] Military Handbook, *Reliability Prediction of Electronic Equipment, Standard MIL-HDBK-217F*, Dec. 1991.

[14] J. Harms, *Revision of MIL-HDBK-217, Reliability Prediction of Electronic Equipment*, 2010.

[15] D. Hirschmann, D. Tissen, S. Schroder, and R. De Doncker, "Reliability prediction for inverters in hybrid electrical vehicles," *IEEE Trans. Power Electron.*, vol. 22, no. 6, pp. 2511–2517, Nov. 2007.

[16] H. S. Chung, H. Wang, F. Blaabjerg, and M. Pecht, "Reliability of power electronic converter systems," Institution Eng. Technol., Stevenage, U.K., 2015.

[17] K. Ma, M. Liserre, F. Blaabjerg, and T. Kerekes, "Thermal loading and lifetime estimation for power device considering mission profiles in wind power converter," *IEEE Trans. Power Electron.*, vol. 30, no. 2, pp. 590–602, Feb. 2015.

[18] Y. Yang, H. Wang, F. Blaabjerg, and K. Ma, "Mission profile based multi-disciplinary analysis of power modules in single-phase transformerless photovoltaic inverters," in *Proc. 15th Eur. Conf. Power Electron. Appl.*, 2013, pp. 1–10.

[19] D. Zhou, F. Blaabjerg, M. Lau, and M. Tonnes, "Optimized reactive power flow of DFIG power converters for better reliability performance considering grid codes," *IEEE Trans. Ind. Electron.*, vol. 62, no. 3, pp. 1552–1562, Mar. 2015.

[20] A. Khosroshahi, M. Abapour, and M. Sabahi, "Reliability evaluation of conventional and interleaved DC–DC boost converters," *IEEE Trans. Power Electron.*, vol. 30, no. 10, pp. 5821–5828, Oct. 2015.

[21] A. M. Bazzi, A. Dominguez-Garcia, and P. T. Krein, "Markov reliability modeling for induction motor drives under field-oriented control," *IEEE Trans. Power Electron.*, vol. 27, no. 2, pp. 534–546, Feb. 2012.

[22] M. Tanrioven and M. S. Alam, "Reliability modeling and analysis of stand-alone PEM fuel cell power plants," *Renewable Energy*, vol. 31, no. 7, pp. 915–933, 2006.

[23] X. Yu and A. M. Khambadkone, "Reliability analysis and cost optimization of parallel-inverter system," *IEEE Trans. Ind. Electron.*, vol. 59, no. 10, pp. 3881–3889, Oct. 2012.

[24] F. Richardeau and T. T. L. Pham, "Reliability calculation of multilevel converters: Theory and applications," *IEEE Trans. Ind. Electron.*, vol. 60, no. 10, pp. 4225–4233, Oct. 2013.

[25] P. Latevi and R. Kouta, "Fault tree analysis for PEM fuel cell degradation process modelling," *Int. J. Hydrogen Energy*, vol. 36, no. 19, pp. 12393–12405, 2011.

[26] D. Zhou, H. Wang, F. Blaabjerg, S. K. Kaer, and D. Blom-Hansen, "System-level reliability assessment of power stage in fuel cell application," in *Proc. IEEE Energy Convers. Congr. Expo*., 2016, pp. 1–8.

[27] D. Zhou, H. Wang, and F. Blaabjerg, "Lifetime estimation of electrolytic capacitors in a fuel cell power converter at various confidence levels," in *Proc. IEEE 2nd Annu. Southern Power Electron. Conf.*, 2016, pp. 1–6.

[28] ReliaSoft Corporation, "System analysis reference," 2015. [Online]. Available: http://reliawiki.org/index.php

[29] L. P. Petersen, L. C. Jensen, and M. N. Larsen, "High efficiency isolated DC/DC converter inherently optimized for fuel cell applications," in *Proc. 15th Eur. Conf. Power Electron. Appl.*, 2013, pp. 1–10.

[30] W. Feng, F. C. Lee, P. Mattavelli, and D. Huang, "A universal adaptive driving scheme for synchronous rectification in LLC resonant converters," *IEEE Trans. Power Electron.*, vol. 27, no. 8, pp. 3775–3781, Aug. 2012.

[31] D. Zhou, H. Wang, F. Blaabjerg, S. K. Kaer, and D. Blom-Hansen, "Real mission profile based lifetime estimation of fuel-cell power converter," in *Proc. IEEE 8th Int. Power Electron. Motion Control Conf.*, pp. 2798–2805, 2016.

[32] Infineon Application Note, "MOSFET power losses calculation using the datasheet parameters," 2006.

[33] International Rectifier Corporation, "Understanding and using power MOSFET reliability data," 1987.

[34] A. Testa, S. De Caro, and S. Russo, "A reliability model for power MOSFETs working in avalanche mode based on an experimental temperature distribution analysis," *IEEE Trans. Power Electron.*, vol. 27, no. 6, pp. 3093–3100, Jun. 2012.

[35] ABB Application Note, "Load-cycling capability of HiPak IGBT modules," Application Note 5SYA 2043-04, 2012.

[36] R. Bayerer, T. Hermann, T. Licht, J. Lutz, and M. Feller, "Model for power cycling lifetime of IGBT modules—various factors influencing lifetime," in *Proc. Integr. Power Syst.*, 2008, pp. 1–6.

[37] R. Amro, J. Lutz, and A. Lindemann, "Power cycling with high temperature swing of discrete components based on different technologies," in *Proc. Power Electron. Specialists Conf.*, 2004, pp. 2593–2598.

[38] M. A. Miner, "Cumulative damage in fatigue," *J. Appl. Mechanics*, no. 12, pp. 159–164, 1945.
[39] H. C. Yildirim, G. Marquis, and Z. Barsoum, "Fatigue assessment of high frequency mechanical impact (HFMI)-improved fillet welds by local approaches," *Int. J. Fatigue*, vol. 52, pp. 57–67, 2013.
[40] P. D. Reigosa, H. Wang, Y. Yang, and F. Blaabjerg, "Prediction of bond wire fatigue of IGBTs in a PV Inverter under a long-term operation," *IEEE Trans. Power Electron.*, vol. 31, no. 10, pp. 7171–7182, Oct. 2016.
[41] ReliaSoft Corporation, "Life data analysis reference," 2015. [Online]. Available: http://reliawiki.org/index.php/Life_Data_Analysis_Reference_Book
[42] H. Wang and F. Blaabjerg, "Reliability of capacitors for DC-link applications in power electronic converters—An overview," *IEEE Trans. Ind. Appl.*, vol. 50, no. 5, pp. 3569–3578, Sep. 2014.
[43] A. Albertsen, "Electrolytic capacitor lifetime estimation," 2016. [Online]. Available: www.jianghai-america.com

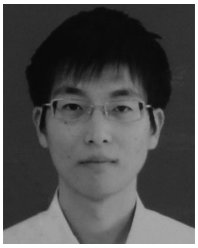

Dao Zhou (S'12–M'15) received the B.S. degree in electrical engineering from Beijing Jiaotong University, Beijing, China, in 2007, the M.S. degree in power electronics from Zhejiang University, Hangzhou, China, in 2010, and the Ph.D. degree in power electronics from Aalborg University, Aalborg, Denmark, in 2014.

He is currently a Postdoctoral Researcher in Aalborg University. His research interests include power electronics and reliability in renewable energy applications.

Dr. Zhou's paper on Renewable and Sustainable Energy Conversion Systems received the First Prize Paper Award of the IEEE Industry Applications Society in 2015. He received the Best Session Paper Award at the annual conference of the IEEE Industrial Electronics Society in 2013 in Austria. He serves as a Session Chair for various technical conferences.

Huai Wang (M'12–SM'17) received the B.E. degree in electrical engineering from Huazhong University of Science and Technology, Wuhan, China, in 2007 and the Ph.D. degree in power electronics from the City University of Hong Kong, Hong Kong, in 2012.

He is currently an Associate Professor and a Research Thrust Leader in the Center of Reliable Power Electronics, Aalborg University, Aalborg, Denmark. He was a Visiting Scientist with the ETH Zurich, Switzerland, from August to September 2014, and with the Massachusetts Institute of Technology (MIT), Cambridge, MA, USA, from September to November 2013. He was with the ABB Corporate Research Center, Switzerland, in 2009. His research addresses the fundamental challenges in modeling and validation of power electronic component failure mechanisms, and application issues in system-level predictability, condition monitoring, circuit architecture, and robustness design. He has contributed a few concept papers in the area of power electronics reliability, filed four patents on capacitive dc-link inventions, and co-edited a book.

Dr. Wang received the Richard M. Bass Outstanding Young Power Electronics Engineer Award from the IEEE Power Electronics Society in 2016, and the Green Talents Award from the German Federal Ministry of Education and Research in 2014. He is currently the Award Chair of the Technical Committee of the High Performance and Emerging Technologies, IEEE Power Electronics Society. He serves as an Associate Editor of *IET Power Electronics*, the IEEE JOURNAL OF EMERGING AND SELECTED TOPICS IN POWER ELECTRONICS, and the IEEE TRANSACTIONS ON POWER ELECTRONICS.

Frede Blaabjerg (S'86–M'88–SM'97–F'03) received the Ph.D. degree in electrical engineering from Aalborg University, Aalborg, Denmark, in 1995.

He was with ABB-Scandia, Randers, Denmark, from 1987 to 1988. He became an Assistant Professor in 1992, an Associate Professor in 1996, and a Full Professor of power electronics and drives in 1998. In 2017, he became a Villum Investigator. His current research interests include power electronics and its applications such as in wind turbines, PV systems, reliability, harmonics, and adjustable speed drives. He has published more than 500 journal papers in the fields of power electronics and its applications. He is the coauthor of two monographs and editor of 6 books in power electronics and its applications.

Dr. Blaabjerg has received 24 IEEE Prize Paper Awards, the IEEE PELS Distinguished Service Award in 2009, the EPE-PEMC Council Award in 2010, the IEEE William E. Newell Power Electronics Award 2014, and the Villum Kann Rasmussen Research Award 2014. He was the Editor-in-Chief of the IEEE TRANSACTIONS ON POWER ELECTRONICS from 2006 to 2012. He has been a Distinguished Lecturer for the IEEE Power Electronics Society from 2005 to 2007 and for the IEEE Industry Applications Society from 2010 to 2011 as well as 2017 to 2018. He was nominated in 2014, 2015, 2016, and 2017 by Thomson Reuters to be between the most 250 cited researchers in engineering in the world. In 2017, he became Honoris Causa at University Politehnica Timisoara (UPT), Romania.